NAVAL POSTGRADUATE SCHOOL
Monterey, California

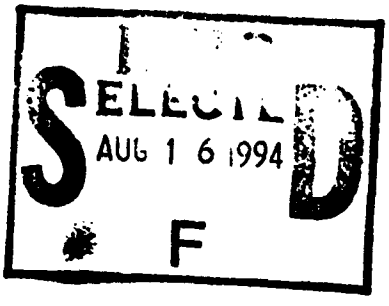

THESIS

THREE-DIMENSIONAL EFFECTS OF CRACK CLOSURE IN LAMINATED COMPOSITE PLATES SUBJECTED TO BENDING LOADS

by

Mehmet Baskaya

June, 1994

Thesis Advisor: Young W. Kwon

REPORT DOCUMENTATION PAGE

Form Approved OMB No. 0704-0188

1. AGENCY USE ONLY	2. REPORT DATE June 1994	3. REPORT TYPE AND DATES COVERED Master's Thesis

4. TITLE AND SUBTITLE THREE-DIMENSIONAL EFFECTS OF CRACK CLOSURE IN LAMINATED COMPOSITE PLATES SUBJECTED TO BENDING LOADS (UNCLASSIFIED)

5. FUNDING NUMBERS

6. AUTHOR(S) Mehmet Baskaya

7. PERFORMING ORGANIZATION NAME(S) AND ADDRESS(ES)
Naval Postgraduate School
Monterey CA 93943-5000

8. PERFORMING ORGANIZATION REPORT NUMBER

9. SPONSORING/MONITORING AGENCY NAME(S) AND ADDRESS(ES)

10. SPONSORING/MONITORING AGENCY REPORT NUMBER

11. SUPPLEMENTARY NOTES The views expressed in this thesis are those of the author and do not reflect the official policy or position of the Department of Defense or the U.S. Government.

12a. DISTRIBUTION/AVAILABILITY STATEMENT
Approved for public release; distribution is unlimited.

12b. DISTRIBUTION CODE
*A

13. ABSTRACT

Fracture is one of the dominant failure modes in structures subjected to external loads. Stress and deformation fields around the crack tip are important to understand the crack propogation and arrest. For a plate with a through-the-thickness crack and subjected to a bending load, there is crack closure on the compression side of the crack face. The present study investigates effects of crack closure on the stress and deformation fields on the tension side of the crack face. A three-dimensional finite element analysis is performed for laminated composite plates using both the line and surface crack closure models. For a composite whose longitudinal elastic modulus is much greater than the transverse modulus, line and surface closure models result in higher stresses near the crack tip in comparison to the no-closure solution. Hence, no-closure solutions are nonconservative for the composite. Transverse shear is the major cause for the nonconservative solution.

14. SUBJECT TERMS FINITE ELEMENT METHOD, BOUNDARY CONDITIONS, CRACK CLOSURE MODELING			15. NUMBER OF PAGES 46 16. PRICE CODE
17. SECURITY CLASSIFICATION OF REPORT Unclassified	18. SECURITY CLASSIFICATION OF THIS PAGE Unclassified	19. SECURITY CLASSIFICATION OF ABSTRACT Unclassified	20. LIMITATION OF ABSTRACT UL

NSN 7540-01-280-5500

Standard Form 298 (Rev. 2-89)
Prescribed by ANSI Std. 239-18

Approved for public release; distribution is unlimited.

Three-Dimensional Effects of Crack Closure in Laminated Composite Plates Subjected to Bending Loads

by

Mehmet Baskaya
Lieutenant Junior Grade, Turkish Navy
B.S., Turkish Naval Academy, 1988

Submitted in partial fulfillment
of the requirements for the degree of

MASTER OF SCIENCE IN MECHANICAL ENGINEERING

from the

NAVAL POSTGRADUATE SCHOOL
June 1994

Author: M. Baskaya
Mehmet Baskaya

Approved by: Young W. Kwon
Young W. Kwon, Thesis Advisor

Matthew D. Kelleher
Matthew D.Kelleher, Chairman
Department of Mechanical Engineering

ABSTRACT

Fracture is one of the dominant failure modes in structures subjected to external loads. Stress and deformation fields around the crack tip are important to understand the crack propogation and arrest. For a plate with a through-the-thickness crack and subjected to a bending load, there is crack closure on the compression side of the crack face. The present study investigates effects of crack closure on the stress and deformation fields on the tension side of the crack face. A three-dimensional finite element analysis is performed for laminated composite plates using both the line and surface crack closure models. For a composite whose longitudinal elastic modulus is much greater than the transverse modulus, line and surface closure models result in higher stresses near the crack tip in comparison to the no-closure solution. Hence, no-closure solutions are nonconservative for the composite. Transverse shear is the major cause for the nonconservative solution.

TABLE OF CONTENTS

I. INTRODUCTION

Plates and shells are very commonly used as structural members in construction of ships and other structures. Due to their wide usage as structural members, much research has been performed to understand their failure mechanisms and modes under different loading conditions. Fracture is one of the most frequent failure modes in plates and shells.

The first analysis on plates containing centrally located through-the-thickness cracks and subjected to bending loads was performed by Williams [Ref. 1] in 1951. In his analysis, Williams used the forth-order classical plate bending theory with Kirchhoff boundary conditions. He showed that there are some discrepencies between the stress distributions for extensional and bending problems. In William's bending study, surface shear stresses on crack faces didn't vanish. This physical violation is attributed to the fact that the Kirchoff bending theory can not satisfy the physical boundary conditions on the crack surface completely.

This problem was solved by Knowles and Wang [Ref. 2]. They used Reissner/Mindlin's sixth order plate theory which allows three boundary conditions at edges. They solved the problem by employing a singular integral equation. However,

their solutions were limited to plates with very small thicknesses. Analyses including effects of the plate thickness on the bending stress distribution were performed independently by Hartranft and Sih [Ref. 3] and Wang [Ref. 4].

All the theories mentioned above assume that the crack surface is stress-free and straight. In reality, for a plate under a bending load, there exists crack closure on the compression side and crack opening on the tension side of the crack surface. A photoelastic experimental study performed by Smith and Smith [Ref. 5] showed partial crack closure. A significant change of local stresses was observed as a result of the crack closure.

A finite element analysis was first undertaken by Jones [Ref. 6] using Kirchhoff's bending theory to study effects of crack closure in plate bending. He compared the closure and no-closure solutions, and reported increases in crack opening displacements and intensity factors due to existing crack closure. In Heming's study [Ref. 7], the Mindlin/Reissner sixth order plate theory was employed, which is more realistic and allows satisfaction of three boundary conditions at the crack face. These results were contradictory to the results obtained by Jones [Ref. 6]. Heming stated that there were significant decreases in the

bending stresses and displacements on the tension side due crack closure.

In those studies, the line closure model, which assumed the outermost points from the neutral axis on the compressive side of the crack surface to be in contact, was used. However, Smith and Smith's experiment [Ref. 5] showed that there was closure over an area of the crack surface, the size of which varied depending on the plate and crack dimensions. A three dimensional finite element analysis was performed by Alwar and Nambissan [Ref. 8] to investigate the closure region and effects on the stress distribution of this closure. A very crude finite element mesh was used in their analyses.

Finally Kwon [Ref. 9] studied the crack closure effect for unidirectional composite plates using the line closure model and the Mindlin/Reissner plate theory. He found that, the crack closure on the compression side of a bent unidirectional composite plate increased the crack opening displacement and bending stress on the tensile side. This finding was in contradiction to that for an isotropic plate. Hence, it was concluded that results obtained without considering crack closure were nonconservative for unidirectional composite plates. The nonconservative solutions for unidirectional composite plates were caused by the effect of transverse shear.

In the present study, effects of surface closure on stresses and displacements around the crack tip in laminated composite plates are investigated using three-dimensional finite element analyses.

II. FINITE ELEMENT FORMULATION

A. OVERVIEW

A finite element program is developed to model a plate with centrally located through-the-thickness crack and subjected to a constant bending load. As shown in Figure 1, the cartesian coordinate system is employed in the model. Displacements in the x, y and z directions are represented by u, v, and w respectively.

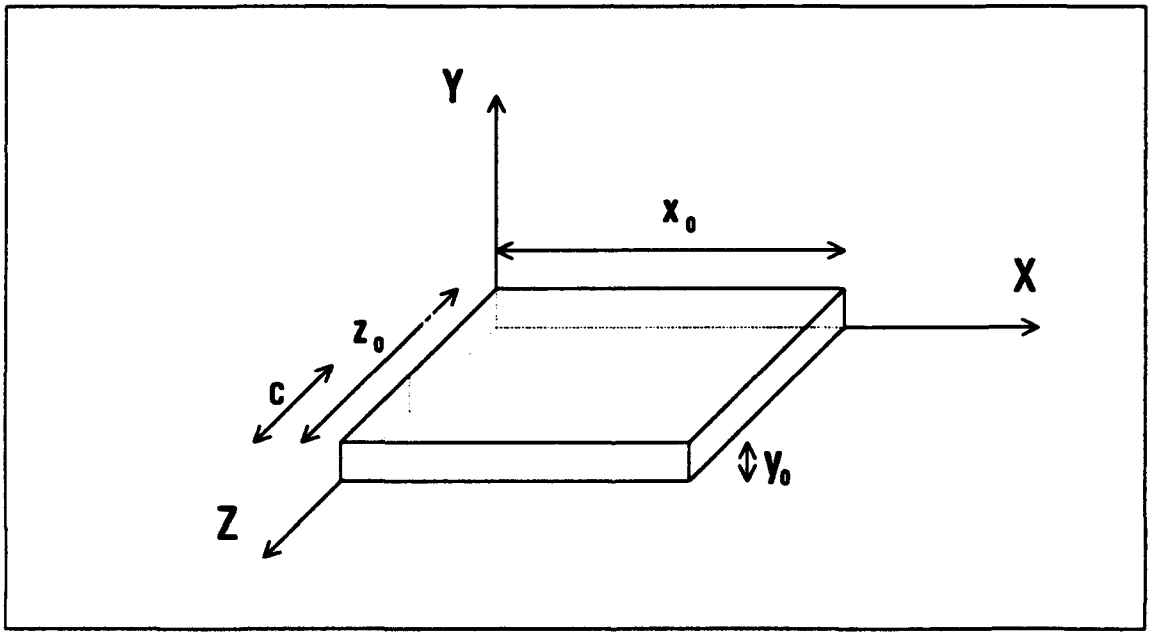

Figure 1 Geometric representation of the plate model

The plate is assumed to have simply supported boundary conditions along its edges. Due to symmetries along the x and z axes, only a quarter of the plate is analyzed to reduce the number of nodes needed in modeling the plate. Therefore, two symmetric boundary conditions and two simply supported boundary conditions are required for the quarter plate. Three-dimensional parallel-piped elements are used in constructing the stiffness matrix. Each node has three degrees of freedom and, therefore, there are 24 dofs per element as shown in Figure 2.

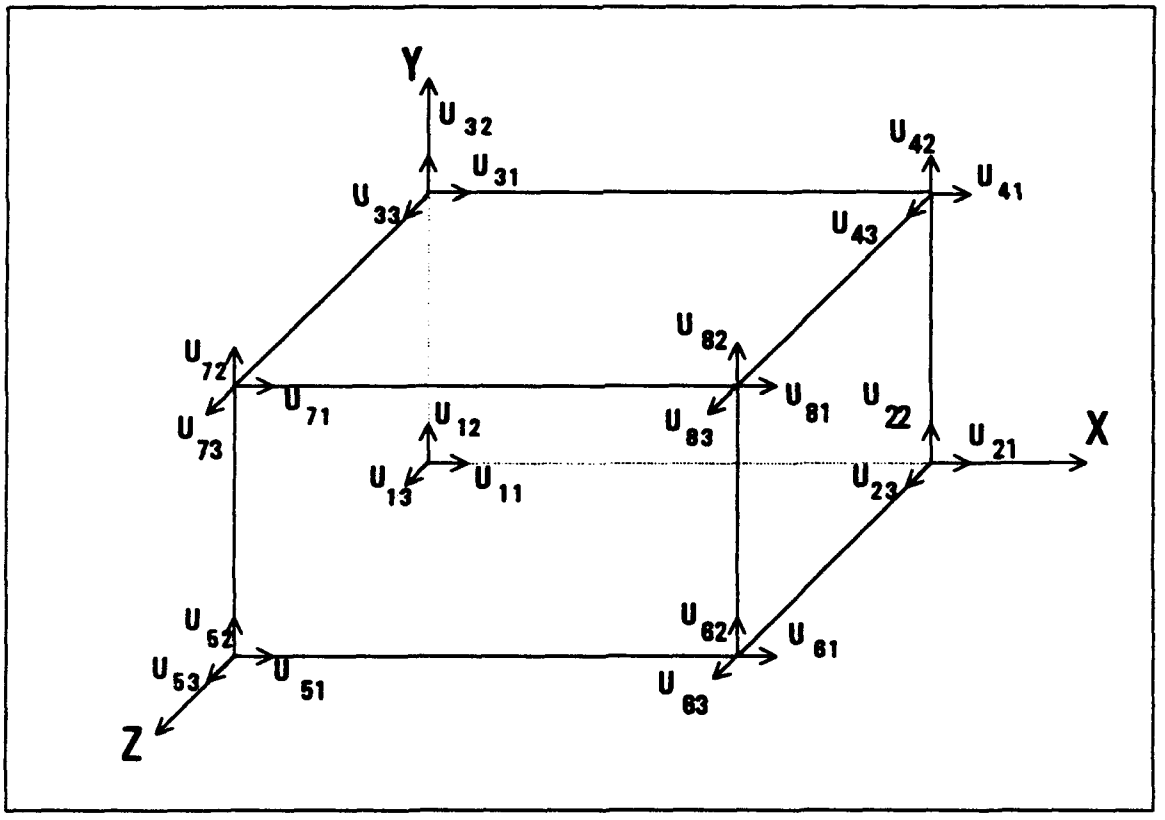

Figure 2 Nodal coordinates of a typical finite element

Displacements of the plate are functions of x, y and z coordinates. That is,

$$u = f_1(x, y, z)$$

$$v = f_2(x, y, z) \tag{1}$$

$$z = f_3(x, y, z)$$

To interpolate the displacements within each finite element, shape functions are utilized. Displacement can be expressed as,

$$u = \sum_{i=1}^{8} N_i * U_{i1} \qquad v = \sum_{i=1}^{8} N_i * U_{i2} \qquad w = \sum_{i=1}^{8} N_i * U_{i3} \tag{2}$$

where subscript i represents the node number, and the numeric subscripts 1, 2, and 3 denote the displacements in the x, y, and z directions, respectively, and N_i is a function of x, y and z.

From the elasticity theory, strains are expressed as given below,

$$e_{xx} = \frac{\partial u}{\partial x} \qquad e_{yy} = \frac{\partial v}{\partial y} \qquad e_{zz} = \frac{\partial w}{\partial z}$$

$$e_{xy} = \frac{\partial u}{\partial y} + \frac{\partial v}{\partial x} \qquad e_{xz} = \frac{\partial u}{\partial z} + \frac{\partial w}{\partial x} \qquad e_{yz} = \frac{\partial v}{\partial z} + \frac{\partial w}{\partial y} \tag{3}$$

When written in the matrix form,

$$\{e\}_{6*1} = [B]_{6*24}\{u\}^{e}_{24*1} \tag{4}$$

where {e} is the strain vector of size 6 by 1, $\{u\}^{e}$ is a nodal displacement vector of size 24 by 1, and [B] is a matrix containing derivatives of the shape functions.

The three-dimensional generalized Hooke's law is defined as,

$$\{\sigma\} = [D]\{\varepsilon\} \tag{5}$$

where [D] is a 6 by 6 material property matrix, and {σ} and {ε} are stress and strain vectors. The stress and strain vectors are written as,

$$\begin{aligned} \{\sigma\} &= [\sigma_{xx}, \sigma_{yy}, \sigma_{zz}, \tau_{xy}, \tau_{xz}, \tau_{yz}]^{T} \\ \{\varepsilon\} &= [\varepsilon_{xx}, \varepsilon_{yy}, \varepsilon_{zz}, \gamma_{xy}, \gamma_{xz}, \gamma_{yz}]^{T} \end{aligned} \tag{6}$$

The elastic strain energy can be written as,

$$E = \frac{1}{2}\int_{V}\{\varepsilon\}^{T}[D]\{\varepsilon\}dV = \frac{1}{2}\int_{V}\{U\}^{T}([B]^{T}[D][B])\{U\}dV \tag{7}$$

In equation (7), only the terms in paranthesis have

dependency on the coordinate system. The volume integral of these terms yields the stiffness matrix,

$$[K]^e = \int_V [B]^T [D][B] dV \tag{8}$$

The equation of static equilibrium for an element can be written as,

$$\{F\}^e = [K]^e \{U\}^e \tag{9}$$

where $\{F\}^e$ is the vector of forces acting on the elemental nodes.

B. CONSTITUTIVE EQUATION

The material property matrix [D] is a symmetric matrix which includes elasticity moduli and Poisson's ratios of the material. In the present work, isotropic, orthotropic and laminated composite plates are examined.

1. ISOTROPIC MATERIAL

There are three independent material constants in the [D] matrix for an isotropic material. Elasticity moduli and Poisson's ratios are the same in every direction. For an isotropic material matrix [D] is given as,

$$\begin{bmatrix} \frac{E*(1-\upsilon)}{(1+\upsilon)*(1-2*\upsilon)} & \frac{E*\upsilon}{(1+\upsilon)*(1-2*\upsilon)} & \frac{E*\upsilon}{(1+\upsilon)*(1-2*\upsilon)} & 0 & 0 & 0 \\ \frac{E*\upsilon}{(1+\upsilon)*(1-2*\upsilon)} & \frac{E*(1-\upsilon)}{(1+\upsilon)*(1-2*\upsilon)} & \frac{E*\upsilon}{(1+\upsilon)*(1-2*\upsilon)} & 0 & 0 & 0 \\ \frac{E*\upsilon}{(1+\upsilon)*(1-2*\upsilon)} & \frac{E*\upsilon}{(1+\upsilon)*(1-2*\upsilon)} & \frac{E*\upsilon}{(1+\upsilon)*(1-2*\upsilon)} & 0 & 0 & 0 \\ 0 & 0 & 0 & G & 0 & 0 \\ 0 & 0 & 0 & 0 & G & 0 \\ 0 & 0 & 0 & 0 & 0 & G \end{bmatrix} \tag{10}$$

2. ORTHOTROPIC MATERIAL

The number of independent material constants in the [D] matrix is six for an orthoropic material. The material properties have three principal axes. The material properties of the plate are considered as, E_1/E_2=5, 20, 40, and 100, G_{12}/E_2=0.6, G_{23}/E_2=0.5, υ_{12}=0.25, and υ_{23}=1/9. Inverse of the [D] matrix is called the compliance matrix and it is given in [Ref. 10] as shown below,

$$\begin{bmatrix} 1/E_1 & -\upsilon_{21}/E_2 & -\upsilon_{31}/E_3 & 0 & 0 & 0 \\ -\upsilon_{12}/E_1 & 1/E_2 & -\upsilon_{32}/E_3 & 0 & 0 & 0 \\ -\upsilon_{13}/E_1 & -\upsilon_{23}/E_2 & 1/E_3 & 0 & 0 & 0 \\ 0 & 0 & 0 & 1/G_{23} & 0 & 0 \\ 0 & 0 & 0 & 0 & 1/G_{31} & 0 \\ 0 & 0 & 0 & 0 & 0 & 1/G_{12} \end{bmatrix} \tag{11}$$

where E denotes inplane elasticity modulus, G denotes shear modulus, and numeric subscripts 1, 2, and 3 represent material principal axes.

3. LAMINATED COMPOSITE MATERIAL

A laminated composite plate with $[0/90]_s$ is investigated. There are two [D] matrices in the model to represent the oriantations of 0 and 90 degrees. The matrix [D] for the 0 degree layer is the same as that for the 90 degree layer except that material properties in the x and z directions (see Figure 1) are interchanged for the 90 degree layer. As a result, the compliance matrix for the 90 degree layer is given below,

$$\begin{bmatrix} 1/E_3 & -\upsilon_{23}/E_2 & -\upsilon_{13}/E_1 & 0 & 0 & 0 \\ -\upsilon_{32}/E_3 & 1/E_2 & -\upsilon_{12}/E_1 & 0 & 0 & 0 \\ -\upsilon_{31}/E_3 & -\upsilon_{21}/E_2 & 1/E_1 & 0 & 0 & 0 \\ 0 & 0 & 0 & 1/G_{21} & 0 & 0 \\ 0 & 0 & 0 & 0 & 1/G_{13} & 0 \\ 0 & 0 & 0 & 0 & 0 & 1/G_{32} \end{bmatrix} \tag{12}$$

C. STRAIN-DISPLACEMENT RELATION

Linear shape functions are utilized in the present finite element formulation. That is,

$$N_1 = \left(\frac{a-x}{a}\right) * \left(\frac{b-y}{b}\right) * \left(\frac{c-z}{c}\right)$$

$$N_2 = \left(\frac{x}{a}\right) * \left(\frac{b-y}{b}\right) * \left(\frac{c-z}{c}\right)$$

$$N_3 = \left(\frac{a-x}{a}\right) * \left(\frac{y}{b}\right) * \left(\frac{c-z}{c}\right)$$

$$N_4 = (\tfrac{x}{a}) * \left(\tfrac{y}{b}\right) * (\tfrac{c-z}{c}) \tag{13}$$

$$N_5 = (\tfrac{a-x}{a}) * \left(\tfrac{b-y}{b}\right) * (\tfrac{z}{c})$$

$$N_6 = (\tfrac{x}{a}) * \left(\tfrac{b-y}{b}\right) * (\tfrac{z}{c})$$

$$N_7 = (\tfrac{a-x}{a}) * \left(\tfrac{y}{b}\right) * (\tfrac{z}{c})$$

$$N_8 = (\tfrac{x}{a}) * \left(\tfrac{y}{b}\right) * (\tfrac{z}{c})$$

where a, b, and c are dimensions of a finite element as seen in Figure 2.

Matrix [B], which relates strains to nodal displacements of an element is formed by taking partial derivatives of the shape functions. Hence, six strain components are expressed as shown below,

$$e_{xx} = \sum_{i=1}^{8} \frac{\partial}{\partial x}[N_i * U_{i1}]$$

$$e_{yy} = \sum_{i=1}^{8} \frac{\partial}{\partial y}[N_i * U_{i2}]$$

$$e_{zz} = \sum_{i=1}^{8} \frac{\partial}{\partial z}[N_i * U_{i3}] \tag{14}$$

$$e_{xy} = \sum_{i=1}^{8} \frac{\partial}{\partial y}[N_i * U_{i1}] + \sum_{i=1}^{8} \frac{\partial}{\partial x}[N_i * U_{i2}]$$

$$e_{xz} = \sum_{i=1}^{8} \frac{\partial}{\partial x}[N_i * U_{i1}] + \sum_{i=1}^{8} \frac{\partial}{\partial x}[N_i * U_{i3}]$$

$$e_{yz} = \sum_{i=1}^{8} \frac{\partial}{\partial x}[N_i * U_{i2}] + \sum_{i=1}^{8} \frac{\partial}{\partial y}[N_i * U_{i3}]$$

D. STIFFNESS MATRIX

The element stiffness matrix $[K]^e$ is found by volume integration of the term ($[B]^T[D][B]$) as in the equation (7), where x varies from 0 to a, ($x \in [o\ a]$)

y varies from 0 to b, ($y \in [o\ b]$)

z varies from 0 to c, ($z \in [o\ c]$)

The global stiffness matrix is constructed by adding element stiffness matrices. In the present finite element mesh, the number of nodes in the x, y, and z directions are 21, 9, and 21 respectively. It gives the halfbandwidth of 636 and total degrees of fredom of 11907. A static pressure load is applied at the nodes ao the xz plane lying in the middle of the plate.

III. BOUNDARY CONDITIONS AND MODELING OF CRACK CLOSURE

Selecting proper constraints imposed along the edges of a plate is very important. As mentioned in [Ref. 7], application of Kirchoff's boundary conditions or Reisner/Mindlin boundary conditions results in contradictory solutions. It is more realistic to employ the Reissner/Mindlin theory, which describes three boundary conditions along the edges of a plate. Therefore, in the present models the Reissner/Mindlin BCs are utilized. Because of the symmetry involved, a quarter of the plate is modeled. The model has two symmetric and two simply supported boundary conditions. Symmetric BCs are satisfied by constraining displacements in the normal direction to the boundary surface. Simply supported boundary conditions, on the other hand are imposed by constraints in vertical displacements and tangential displacements at the boundary surface.

Crack closure is a constraint on the crack face. There are three crack surface models which are used in analyses of plates with through-the-thickness cracks. The first model assumes that the plate has no constraint on the crack surface, as seen in Figure 3a. This is called the

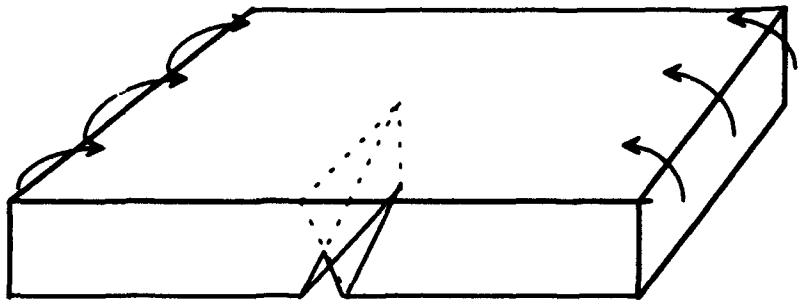

Figure 3a No-Closure Model

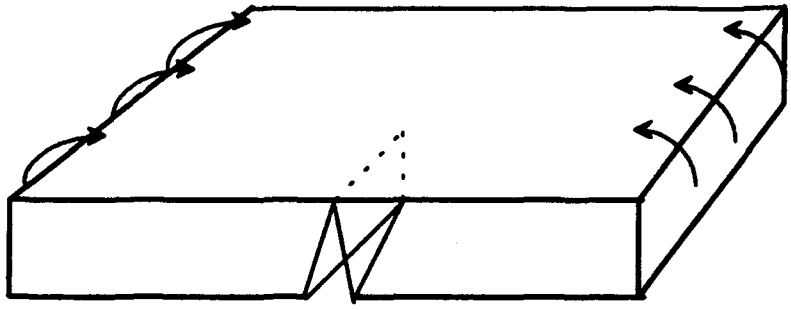

Figure 3b Line Closure Model

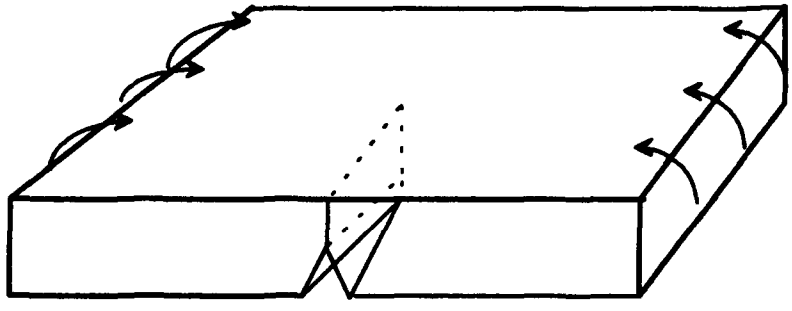

Figure 3c Surface Closure Model

no-closure model. The crack surface is considered as stress-free and straigth .

The assumption of no-closure allows crack opening to occur on the tension side of the crack face. On the other side of the crack face, deformations of the same magnitudes occur in the opposite direction. Hence, overlapping or penetration takes place by employing the no-closure model. However, penetration is not possible in the actual case. In reality, there would be contact over a region on the crack surface. And this contact is called crack closure.

We can model the closure region in two different ways. In the first model the outermost nodes on the compression side with respect to the neutral axis are constrained to avoid penetration. This is called the line closure model and is shown in Figure 3b. Alternatively, a region which contains some of the nodes between the outermost nodes and neutral axis on the compression side of the crack face can be constrained, as shown in Figure 3c. This second model is called the surface closure model.

Plate bending theories permit only the line closure model, because the theories assume that plane sections remain plain before and after bending. The experimental study by Smith and Smith [Ref. 5] shows that crack closure takes place over a portion of the crack face. Therefore, the surface closure model is the closest describtion of the

crack closure. An iteration process is necessary to model surface closure using a contact algorithm. Proper number of nodes are constrained to ensure that there is no penetration on the crack surface.

When using the finite element method, it is possible to model the surface crack closure using 2-D plate bending elements or 3-D solid elements. If 2-D plate bending elements are used in modeling, a stack of plate elements are used through the plate thickness. As a result, the crack face can have a piecewise linear deformation and the closure portion becomes a rectangular shape. With 3-D solid elements, displacements at the crack face can have more general deformation. Hence, a general shape of surface crack closure can be modeled. Because of this advantage, we use 3-D elements in the present study.

IV. RESULTS AND DISCUSSIONS

In the present study, cracked plates made of three kinds of materials are examined. These are isotropic, orthotropic and three layered composite plates with an orientation of [0/90/0]. Four different elasticity moduli ratios, E1/E2=5, 20, 40, and 100, are considered for composite and orthotropic models. Consequently, we analyzed nine models with different material properties. Three types of crack closure modelings, which are discussed in the previous chapter, are employed to model the crack surface. These are surface closure, line closure, and no-closure models. All three models are compared with each other for each cracked plate.

All the stress and displacement data are computed on the plane containing the crack. A three dimensional representation of the crack surface for the no-closure model is shown in Figure 4. In this figure flat section is the uncracked portion of the crack plane. Since for the no-closure model there is no constraint on the crack surface, displacements with the same magnitudes and in the opposite directions are observed on the tension and compression sides. In the surface closure model, due to the

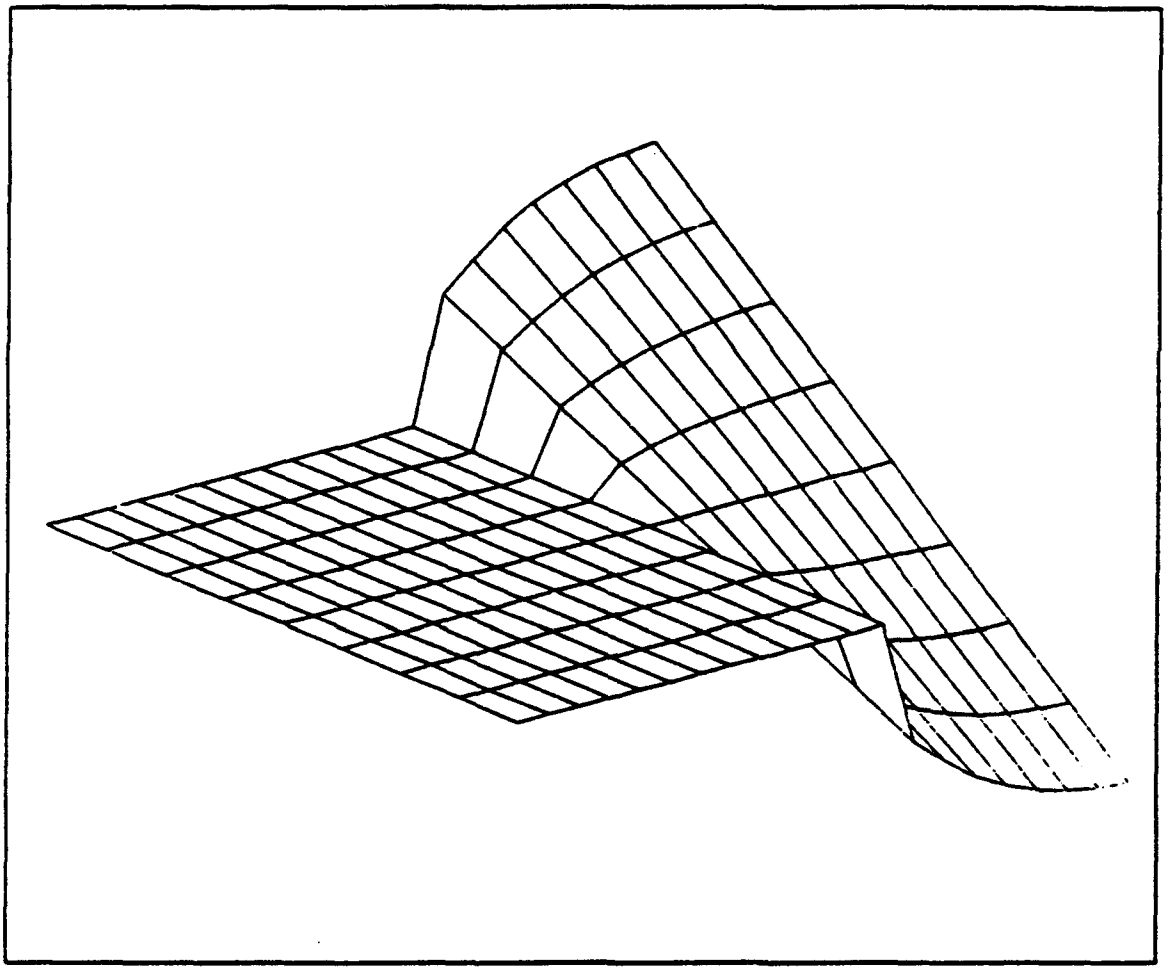

Figure 4 Three Dimensional Representation of the Crack Surface for No-closure model.

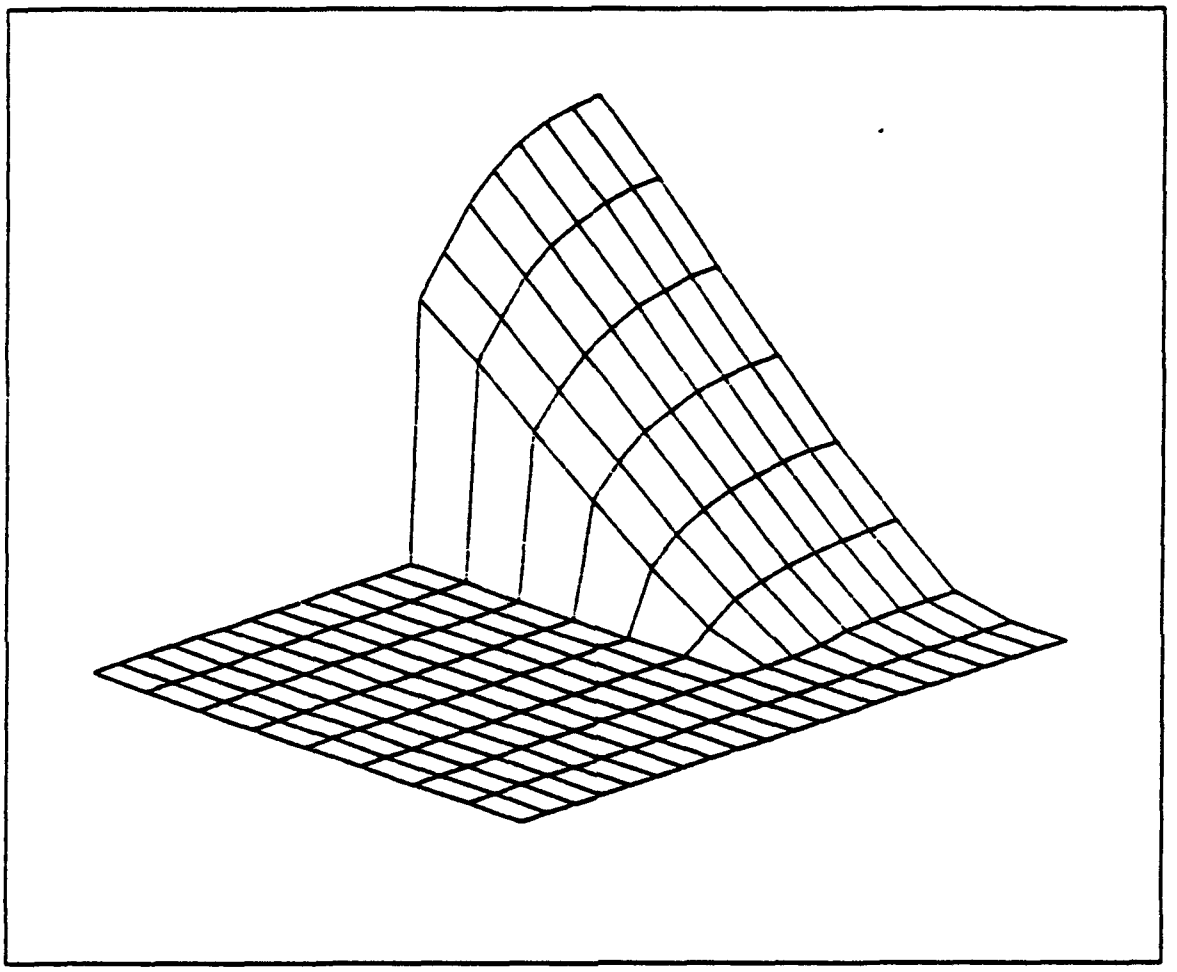

Figure 5 Three Dimensional Representation of the Crack Surface for surface closure model.

crack closure, only displacements in the crack opening direction are allowed, as shown in Figure 5.

Effects of closure on the crack opening displacements can be explained by considering a compressive force due to closure as shown in Figure 6a, that acts on the compression side of the crack surface. A statically equivalent force and moment, as in Figure 6b, can be thought acting in the middle of the plane. While the force increases the crack opening displacements on the entire surface of the crack, the moment causes decreases on the tension side. For smaller elasticity ratios the effect of the moment is greater. Hence, we observe decreases in crack opening displacements. For higher elasticity ratios, especially in the case of a composite plate, the effect of the force is higher.

When the elasticity ratio is higher, shear deformation due to transverse shear becomes more important. As seen in Figure 6c the rotation caused by the moment is decreased due to the transverse shear effect. Here θ is the rotation angle for the moment without considering transverse shear effect, and γ is the rotation angle in the opposite direction due to the transverse shear.

In the displacement plots, the horizontal axis represents the normalized distance from the crack tip and the vertical axis represents crack opening displacements on the tension side of the plate. These crack opening

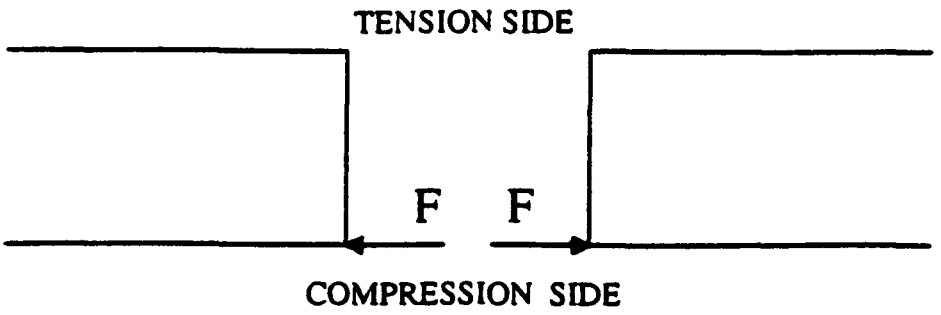

Figure 6a Compressive Force due to Closure

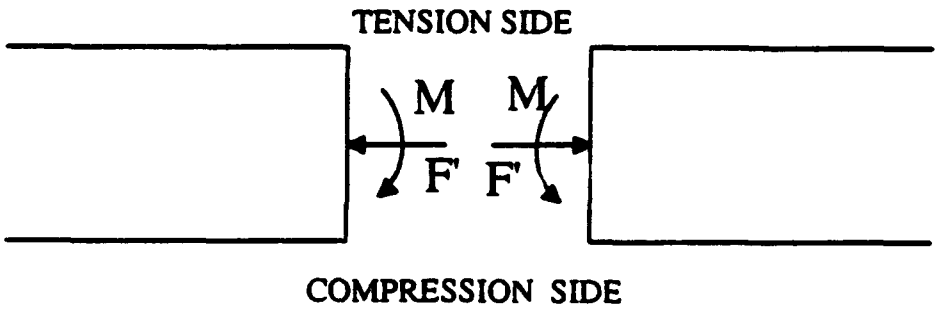

Figure 6b Statically Equivalent Force and Moment

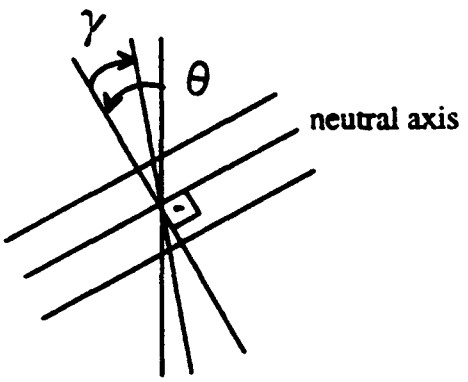

Figure 6c Transverse Shear Effect

displacements (CODs) are normalized by the maximum displacement of the corresponding no closure model. Since there is contact on the compression side for closure models, only displacements on the tension side are plotted.

It is observed that the crack opening displacements for line and surface closure models are very close to each other for all the elasticity ratios. When low elasticity ratios are considered, crack closure decreases the crack opening displacements on the tension side all the way. This is due to the fact that the effect of the moment is higher for low elasticity ratios. Since there are more constraints for the surface closure model its displacements are smaller. Figure 7 shows the crack opening displacements on the tension side of a laminated, cross-ply composite plate with the elasticity ratio E1/E2=5.

From Figure 8 it is seen that, when the elasticity ratio, E1/E2, is 20, crack closure reduces the displacements near the crack tip. On the other hand, it increases the displacements away from the crack tip. When the plots for E1/E2=5 and E1/E2=20 are compared, a slight increase near the crack tip is also observed.

Further inreases in the crack opening displacements are obtained for elasticity ratio E1/E2=40, as seen in Figure 9. Near the crack tip, the displacements for closure cases are still lower than that for the no closure case.

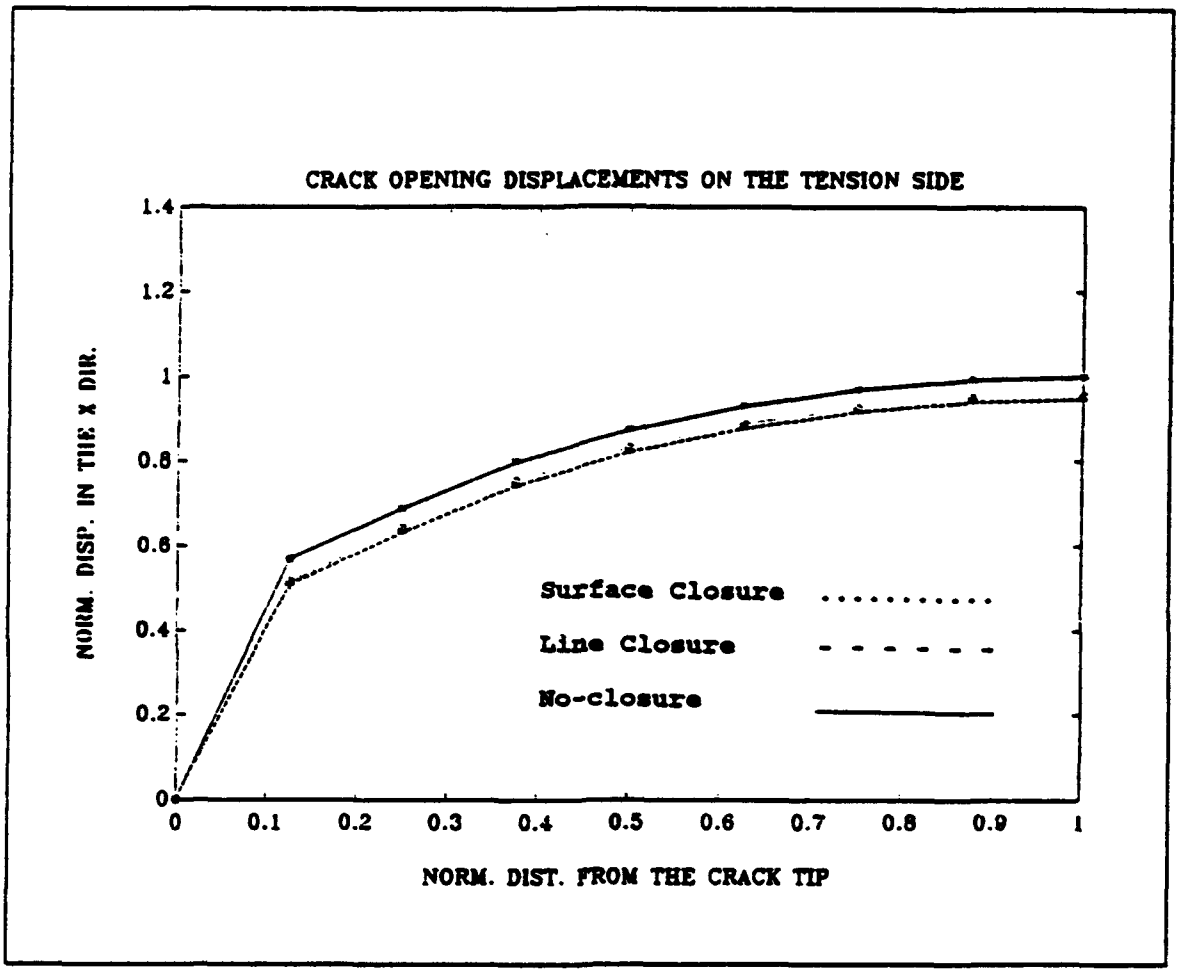

Figure 7 Crack Opening Displacements (CODs) on the tension side of a laminated, cross-ply composite plate with elasticity ratio $E_1/E_2=5$.

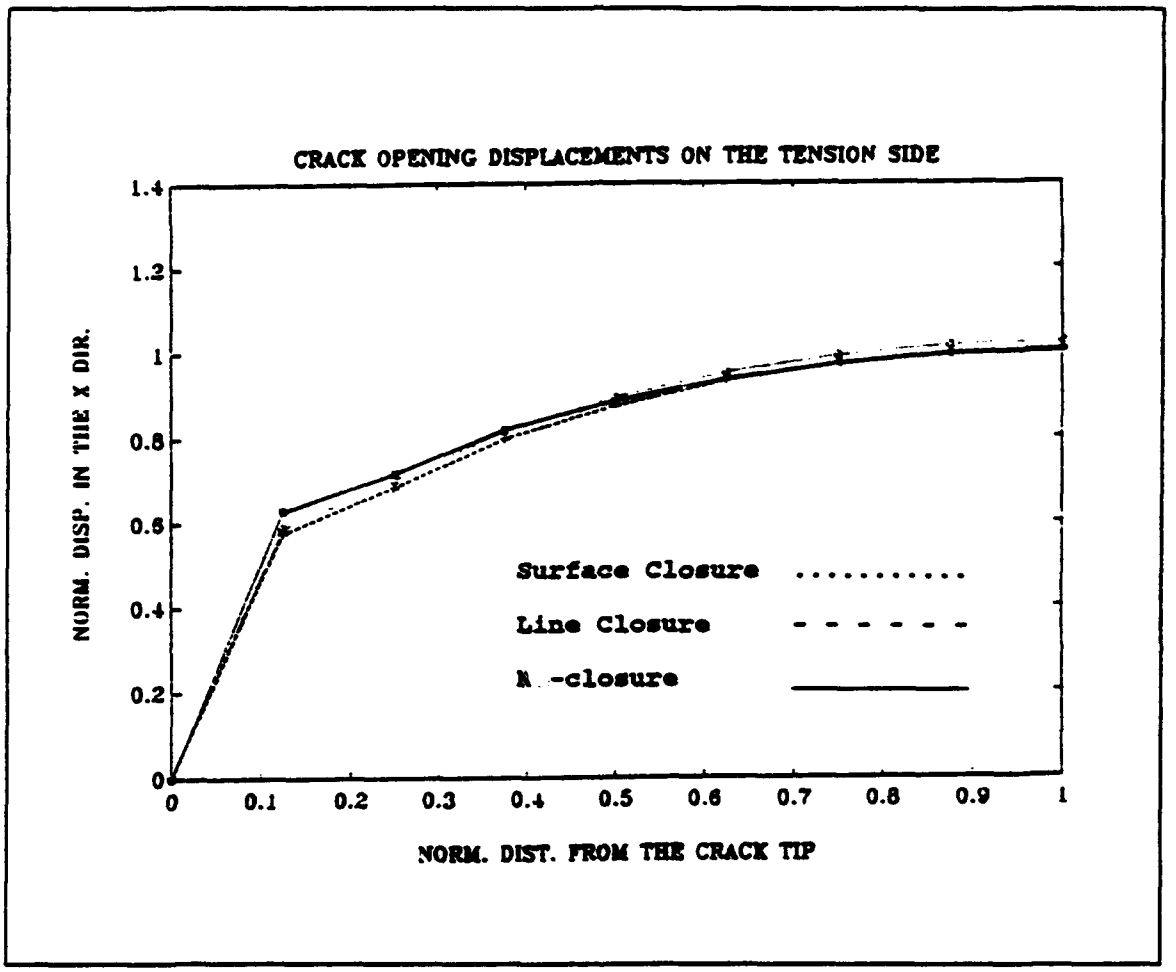

Figure 8 Crack Opening Displacements (CODs) on the tension side of a laminated, cross-ply composite plate with elasticity ratio $E_1/E_2=20$.

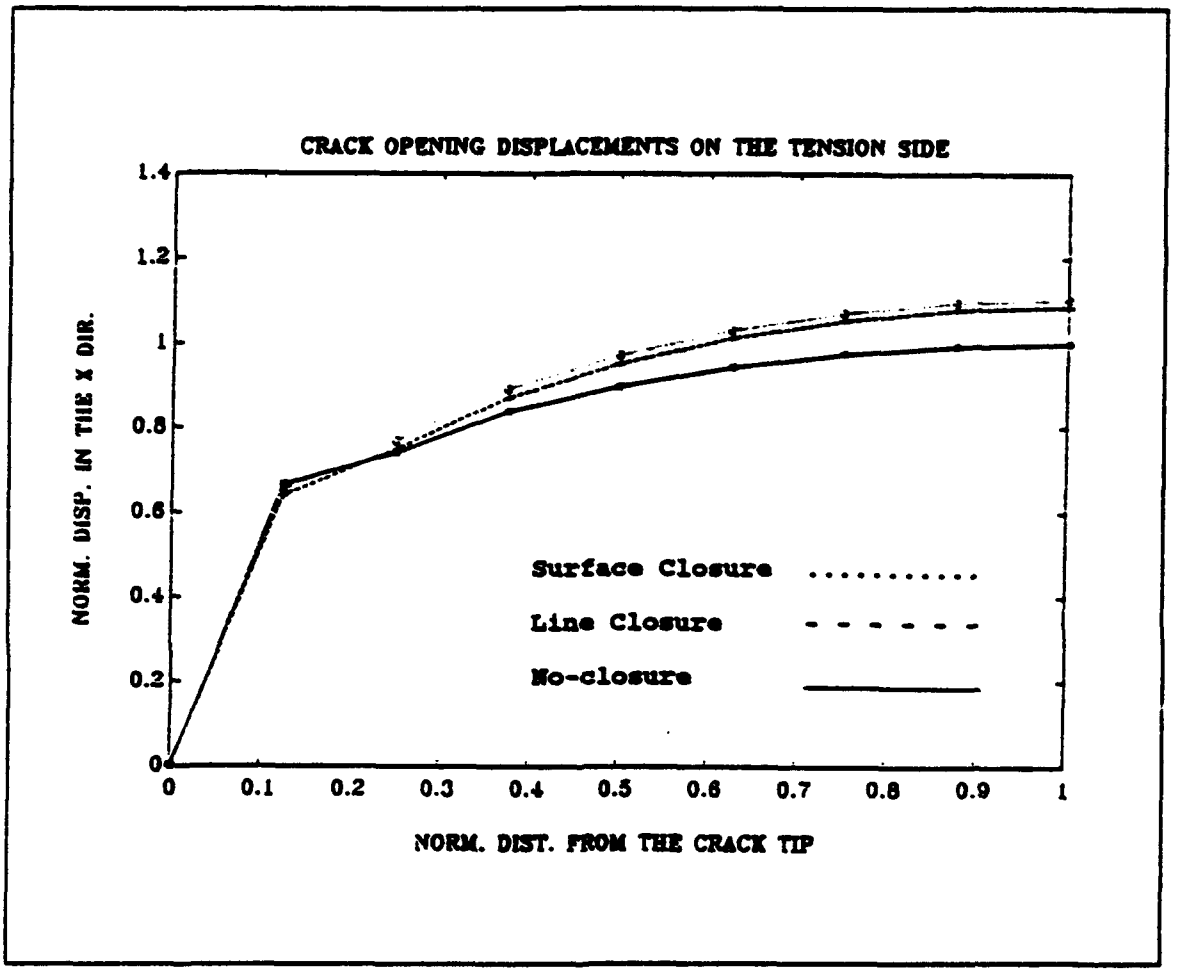

Figure 9 Crack Opening Displacements (CODs) on the tension side of a laminated, cross-ply composite plate with elasticity ratio $E_1/E_2=40$.

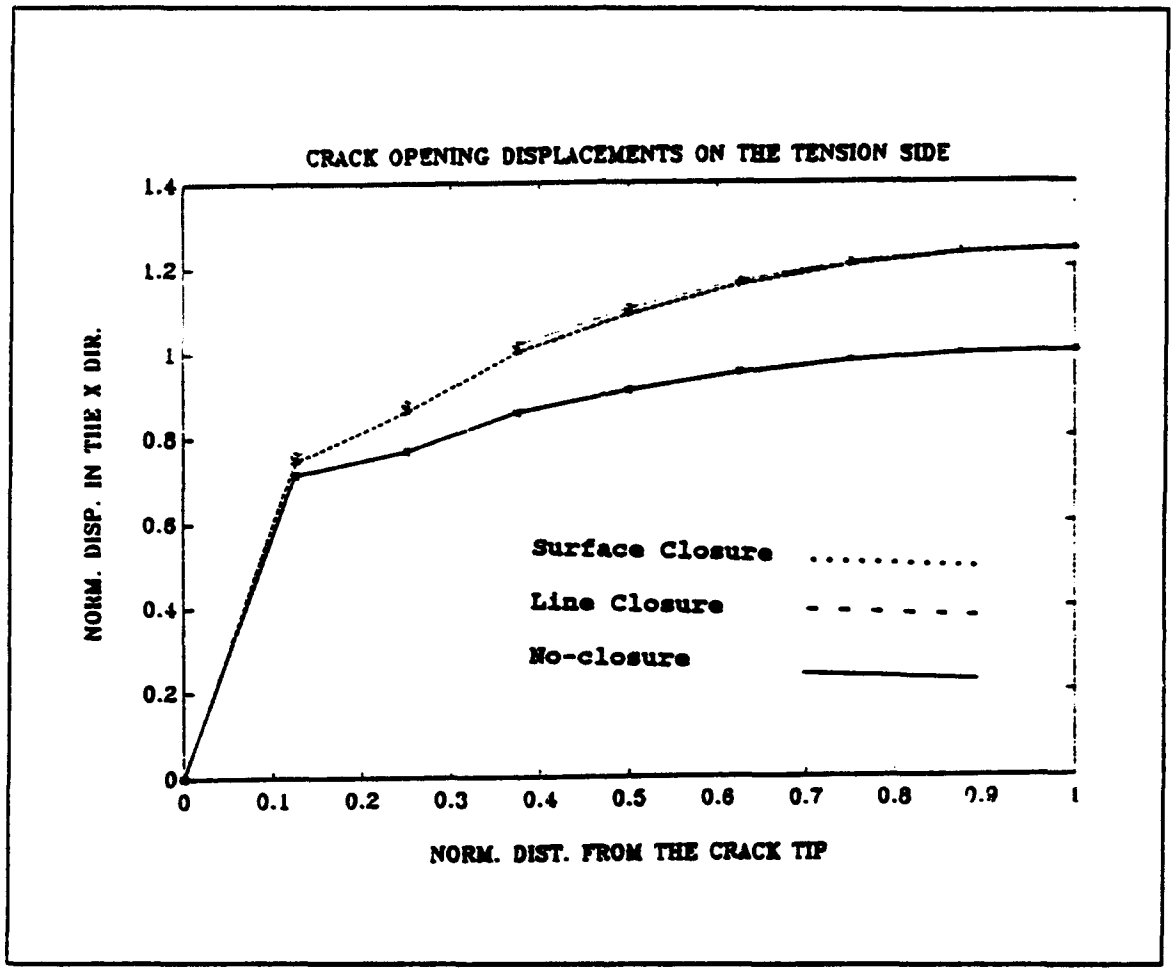

Figure 10 Crack Opening Displacements (CODs) on the tension side of a laminated, cross-ply composite plate with elasticity ratio $E_1/E_2=100$.

When E1/E2=100, closure increases the crack opening displacements all the way, as seen in Figure 10. This is because the transverse shear effect is high enough to overcome the effect of the moment also near the crack tip.

Since the closure cases reduce the stresses on the compression side more, stress distributions on the tension side are different from those on the compression side. Therefore, both tension and compression sides are examined. In the stress plots, the horizontal axis represents the normalized distance from the crack tip upto the corner of the plate along the uncracked portion of the crack plane. The vertical axis represents stresses that are normalized by the applied constant pressure .

From Figures 11 and 12 it can be seen that for E1/E2=5, there exist large discrepencies in the stress levels between closure and no-closure cases. These differences occur both on the tension and the compression sides of the plate. On the other hand, the differences in stresses for surface closure and line closure cases are very small as seen in the crack opening displacements. This is especially true on the tension side.

When higher elasticity ratios are considered, increases in the stresses near the crack tip are observed for closure cases compared to no-closure case, as shown in Figures 13 to

18. When the E1/E2=100, higher stresses are obtained on the tension side for closure cases.

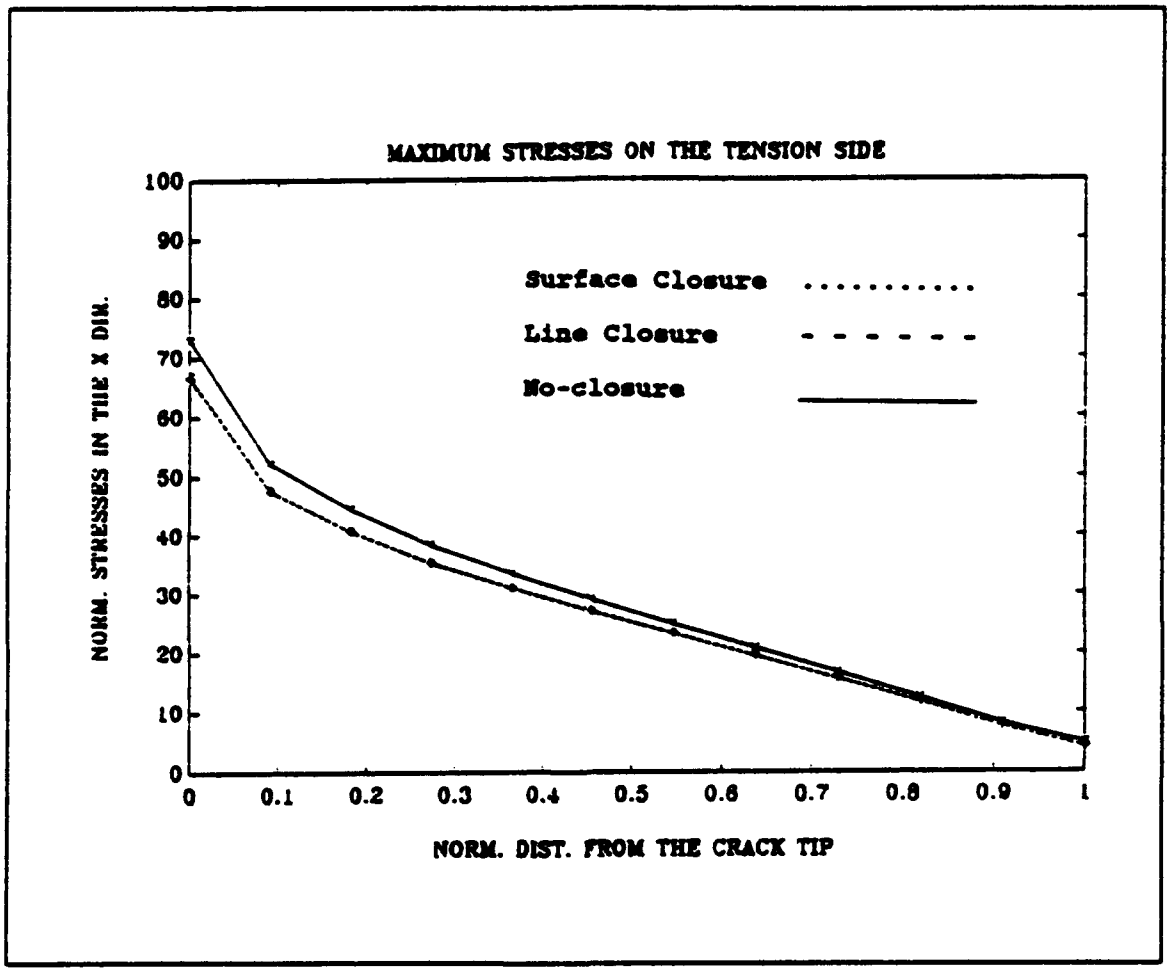

Figure 11 Stress distribution on the tension side of a laminated, cross ply composite plate with elasticity ratio $E_1/E_2=5$.

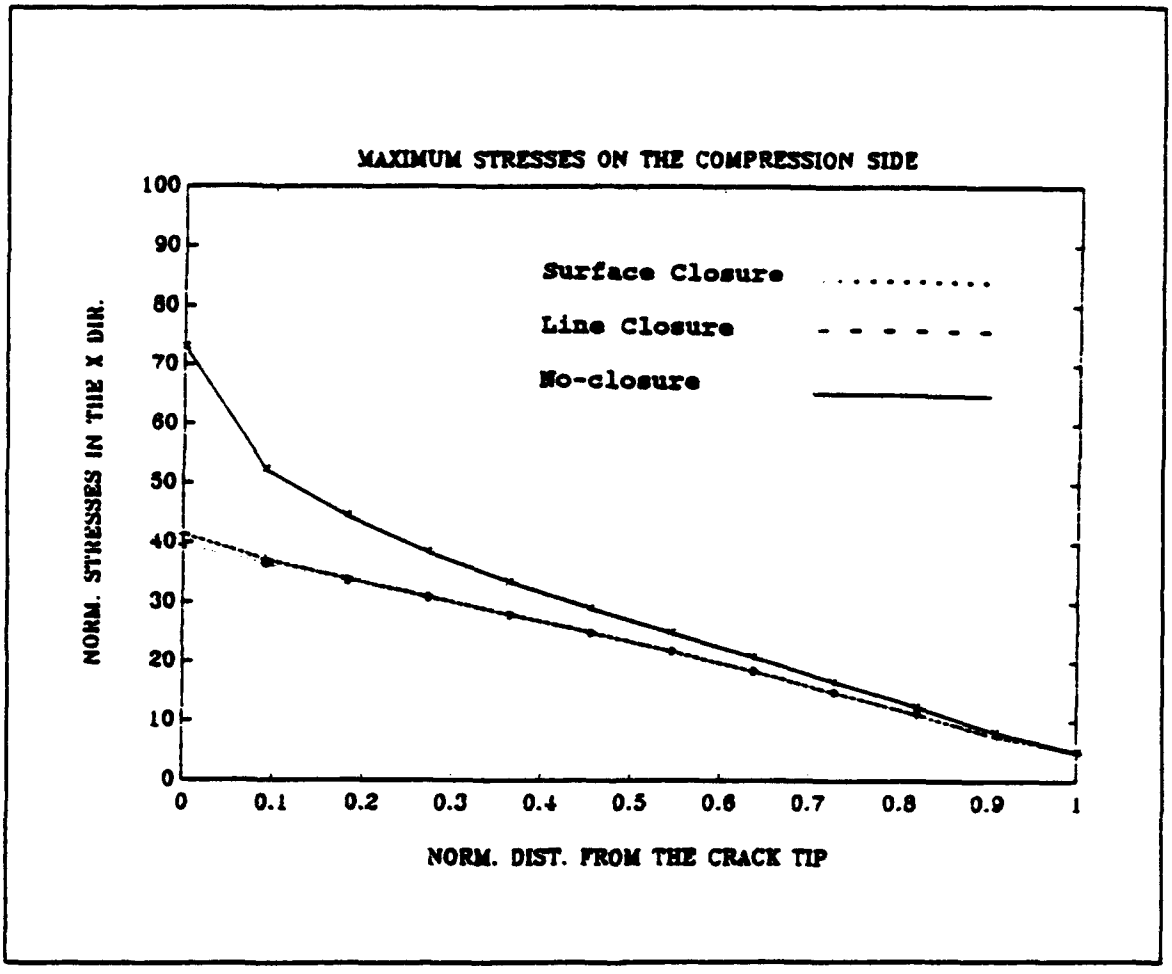

Figure 12 Stress distribution on the compression side of a laminated, cross-ply composite plate with elasticity ratio $E_1/E_2=5$.

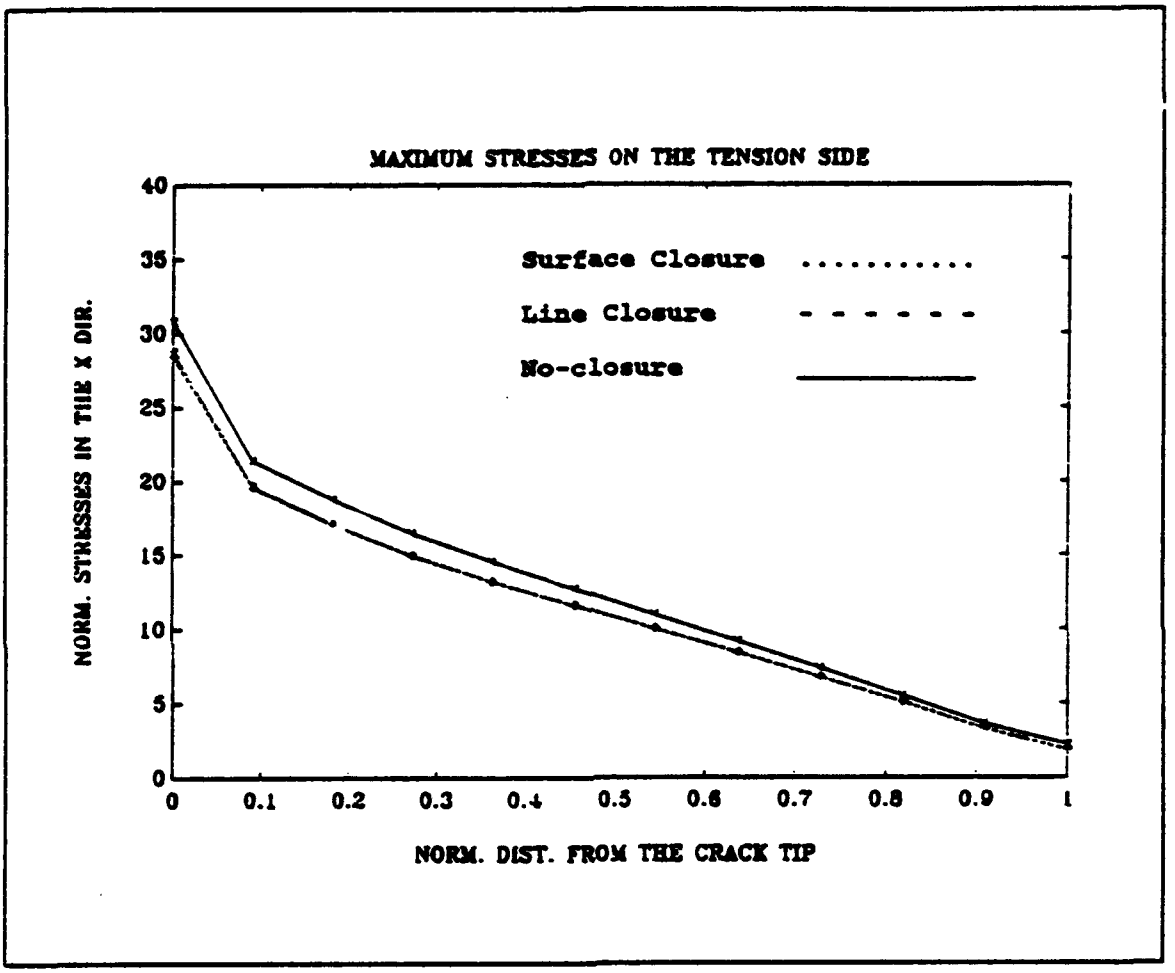

Figure 13 Stress distribution on the tension side of a laminated, cross-ply composite plate with elasticity ratio $E_1/E_2=20$.

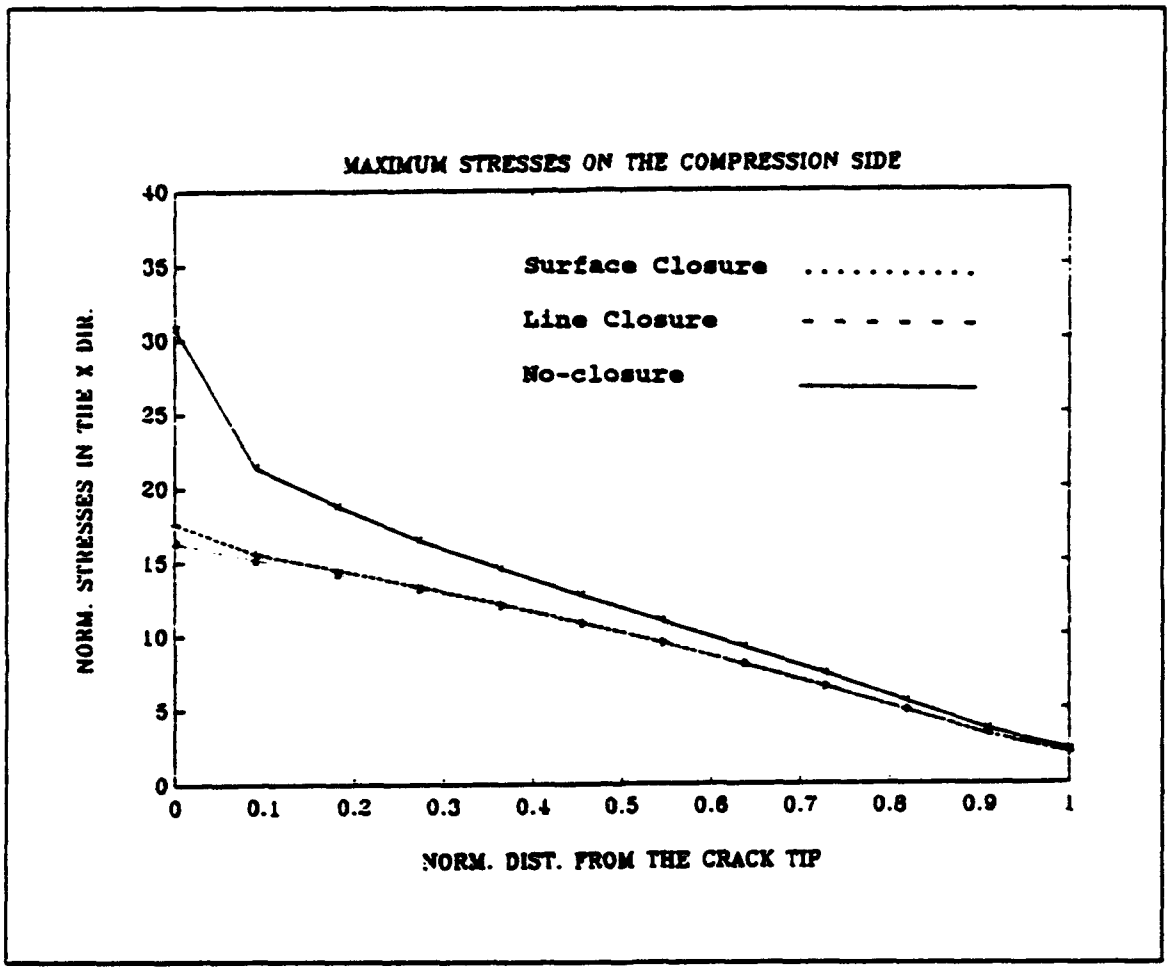

Figure 14 Stress distribution on the compression side of a laminated, cross-ply composite plate with elasticity ratio $E_1/E_2=20$.

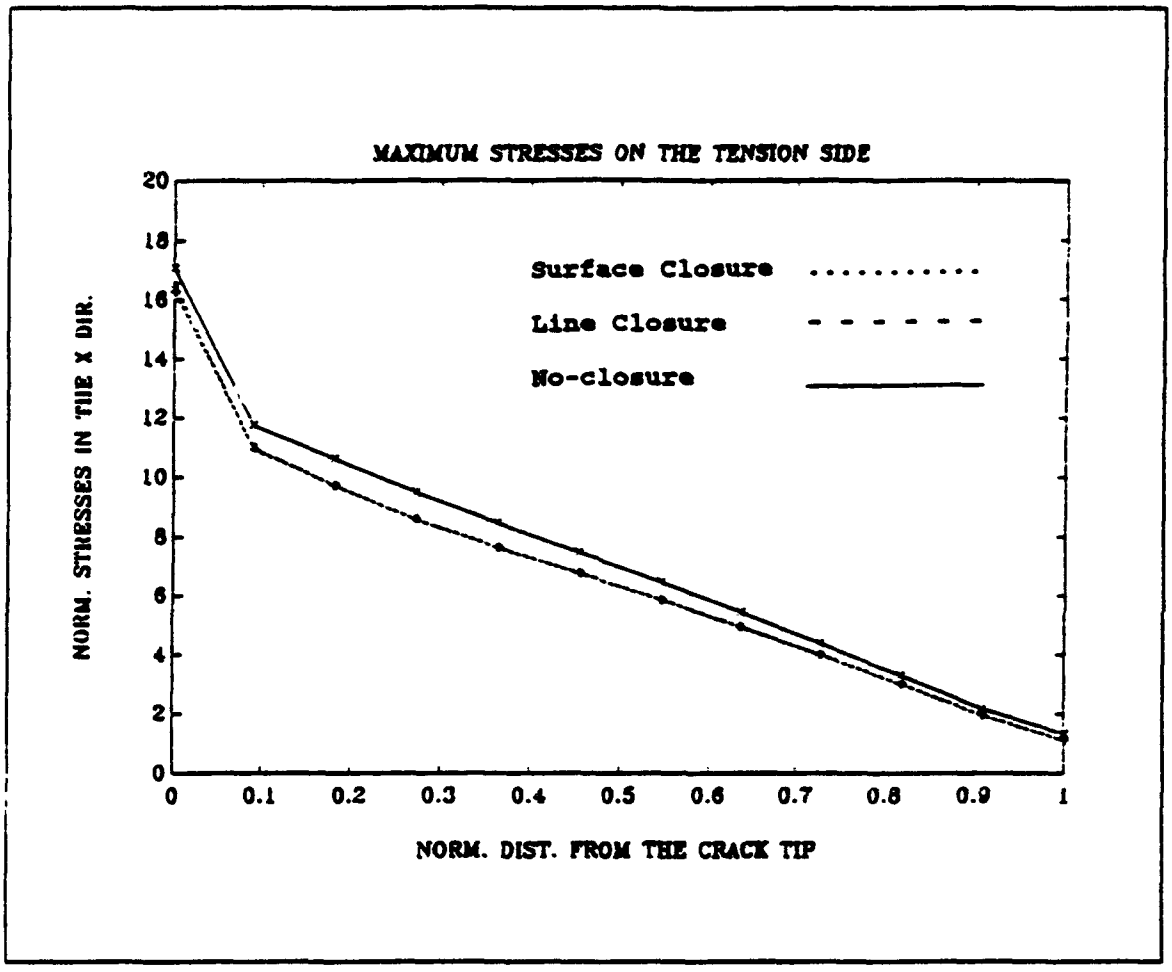

Figure 15 Stress distribution on the tension side of a laminated, cross-ply composite plate with elasticity ratio $E_1/E_2=40$.

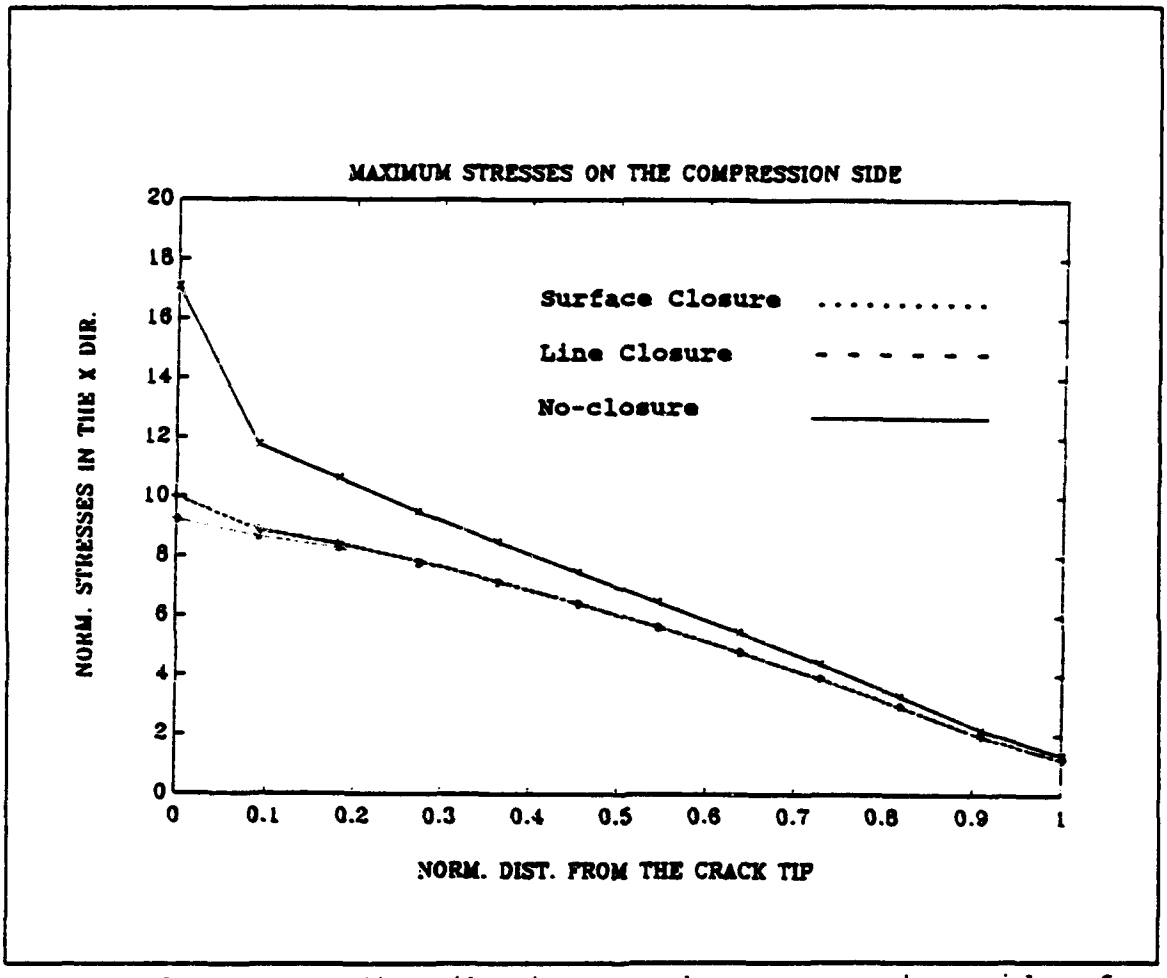

Figure 16 Stress distribution on the compression side of a laminated, cross-ply composite plate with elasticity ratio $E_1/E_2=40$.

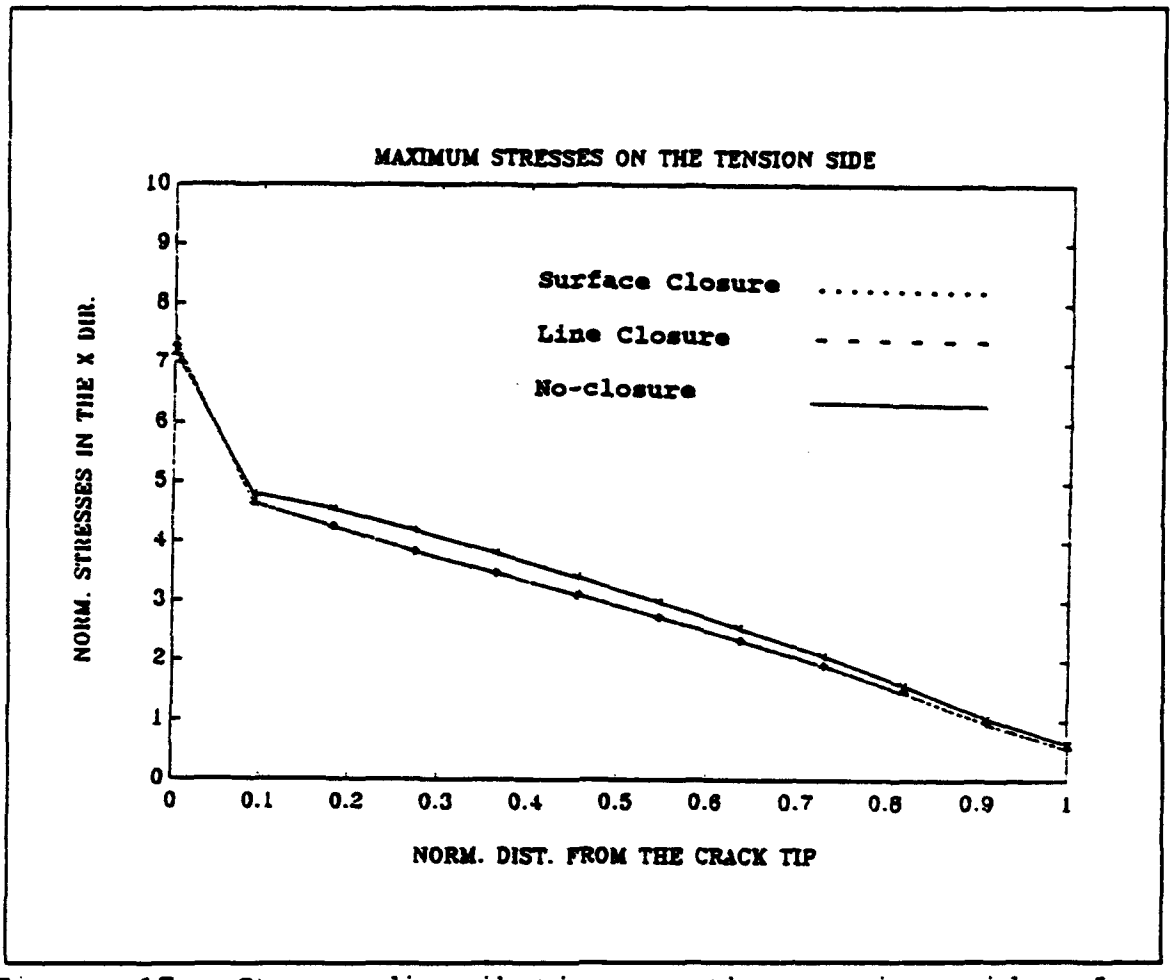

Figure 17 Stress distribution on the tension side of a laminated, cross-ply composite plate with elasticity ratio $E_1/E_2=100$.

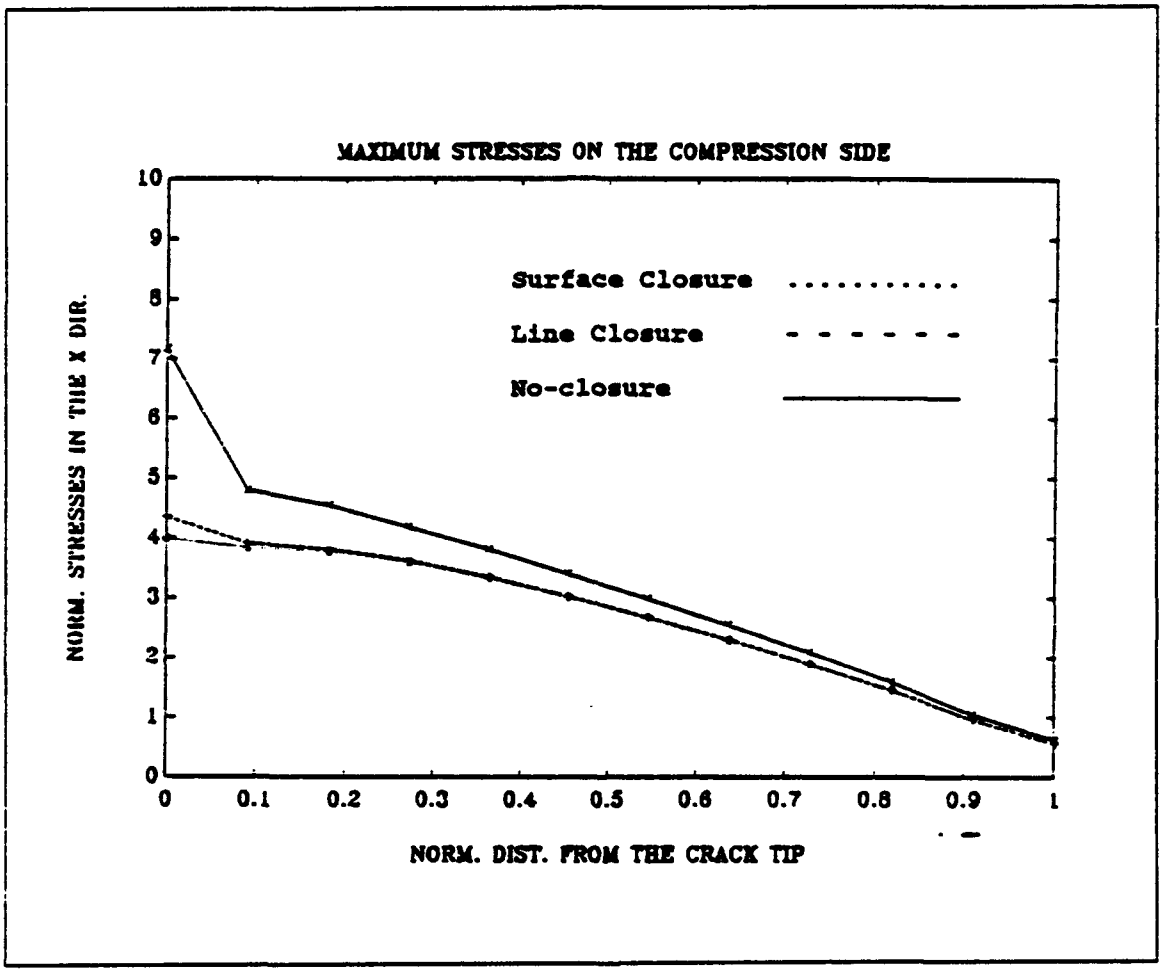

Figure 18 Stress distribution on the compression side of a laminated, cross-ply composite plate with elasticity ratio $E_1/E_2=100$.

V. CONCLUSIONS AND RECOMMENDATIONS

When a laminated composite plate with a through the thickness crack has a large ratio between the longitudinal and transverse elastic moduli, crack closure increases the crack opening displacement and tensile bending stress around the crack tip compared to those obtained without considering crack closure. There is also a slight difference between surface and line closure solutions since the surface closure model has more constraints. Both crack closure solutions are nonconservative. As a result, crack closure must be considered for most composite plates under consideration.

An experimental study shows that the surface closure model is the closest description of crack closure. Since similar displacements and stresses are, however, observed around the crack tip, line closure can be used to model crack closure for computational efficiency.

In future studies experiments may be performed to validate the computer results. Effects of crack closure on composite plates containing delamination cracks need to be analyzed.

LIST OF REFERENCES

1. Williams, M.L., " Proceedings ", First U.S. National Congress of Applied Mechanics, 325-329, 1951.

2. Knowles, J.K. and Wang, N.M., " On the Bending of an Elastic Plate Containing a Crack ", Journal of Mathematics and Physics , 39, No.5, pp.223-236, 1960.

3. Hartranft, R.J. and Sih, G.C., " Effect of Plate Thickness on the Bending Stress Distribution Around Thr gh Cracks ", Journal of Mathematics and Physics, 47, 3, 276-291, 1968.

4. Wang, N.M., " Effect of Plate Thickness on the Bending of an Elastic Plate Containing a Crack ", Journal of Mathematics and Physics, Vol. 47, pp.371-390, 1968.

5. Smith, D.G. and Smith, C.W., " A Photoelastic Evaluation of the Influence of Closure and Other Effects upon the Local Bending Stresses in Cracked Plates ", Int. J. Fracture, 505-318, 1970.

6. Jones, D.P., " Elasto-plastic Bending of Cracked Plates, Including the Effect of Crack Closure ", Ph.d. Thesis, Mechanical Engineering, Carnegie-Mellon Univesity, Report SM-83A, 1972.

7. Heming, F.S. Jr.," Sixth Order Analysis of Crack Closure in Bending of an Elastic Plate ", Int. J. Fracture, 16, 289-304, 1980.

8. Alwar, R.S. and Nambissan, K.N., " Influence of Crack Closure on the Stress Intensity Factor for Plates Subjected to Bending-a 3D finite element analysis ", Engng. Fracture Mech., 17, 323-333, 1983.

9. Kwon, Y.W., " Analysis of Crack Closure in Unidirectional Composite Plates Subject to Bending Loads ", Engng. Fracture Mech., Vol. 42, No5, pp. 825-831,1992.

10. Whitney, J.M., " Structural Analysis of Laminated Anisotropic Plates ", Technomic Publishing Company, Inc., 1987.

INITIAL DISTRIBUTION LIST

		No. Copies
1.	Defense Technical Information Center Cameron Station Alexandria, Virginia 22304-6145	2
2.	Library, Code 52 Naval Postrgaduate School Monterey, California 93943-5101	2
3.	Professor Y.W. Kwon, Code ME/Kw Department of Mechanical Engineering Naval Postgraduate School Monterey, CA 93943-5000	2
4.	Naval Engineering Curricular Office, Code 34 Naval Postgraduate School Monterey, CA 93943-5000	1
5	Department Chairman, Code ME/Kk Department of Mechanical Engineering Naval Postgraduate School Monterey, CA 93943-5000	1
6	Deniz Kuvvetleri Komutanligi Personel Egitim Daire Baskanligi Bakanliklar Ankara Turkey	1
7.	Deniz Harp Okulu Tuzla Istanbul, Turkey	1
8.	Mehmet Baskaya Seyfidemirsoy Mah. Ulutan sok. 194/10 Icaydinlik, Ankara, Turkey	1

9. Istanbul Teknik Universitesi
Universite Kutuphanesi, Beyazit
Istanbul Turkey

1

10. Ortadogu Teknik Universitesi
Universite Kutuphanesi
Ankara, Turkey

1